STUDIA UBB CHEMIA, LX, 2, Tom I, 2015 (p. 27-44)
(RECOMMENDED CITATION)

INFLUENCE OF GRAIN AND CRYSTALLITE SIZE ON THE GIBBSITE TO BOEHMITE THERMAL TRANSFORMATION

VIKTOR ZSOLT BARANYAI[a,b], FERENC KRISTÁLY[c,*], ISTVÁN SZŰCS[a]

ABSTRACT. Thermal decomposition processes of three different samples of hydrated alumina: Bayer precipitated size fractioned, Bayer precipitated ground and fine precipitated, were studied. These were investigated with special regard to evolution of boehmite. The original samples contained 75-85 wt% of gibbsite, while remaining material with gibbsite-like Al_2O_3-H_2O ratio did not show long range order crystallinity. Decomposition reactions were observed by thermal analysis and reaction products were investigated by powder X-ray diffraction. Grain sizes were determined by laser diffraction and morphological changes of grains were observed by scanning electron microscopy. Boehmite formation is influenced mainly by grain and crystallite sizes of starting materials, while degree of crystallinity is of less importance. Transformation of gibbsite to boehmite was most pronounced in the case of coarse grains, nevertheless in fine particles boehmite evolution seemed retarded.

Keywords: *gibbsite decomposition, boehmite evolution, nanocrystalline boehmite, Rietveld-refinement*

INTRODUCTION

Gibbsite (γ–$Al(OH)_3$), end-product of the Bayer cycle is essential raw material of calcined alumina (Al_2O_3). Utilization of aluminum oxide in ceramic technologies has long history [1], however beyond the prevalent technologies, application of gibbsite or boehmite in ceramic green bodies, green fibers has appeared for increasing the final porosity of sintered material [2-4] or stabilizing of alumina foams [5, 6]. In this case the chemically bound water content of raw material is removed during sintering.

[a] *University of Miskolc, Department of Combustion Technology and Thermal Energy, H-3515 Miskolc-Egyetemváros, Hungary*
[b] *Bay Zoltán Nonprofit Ltd. for Applied Research, Department of Advanced Materials, H-3519 Miskolc, Iglói út 2.*
[c] *University of Miskolc, Institute of Mineralogy and Geology, H-3515 Miskolc-Egyetemváros, Hungary*
[*] *Corresponding author: kristalyf@gmail.com*

The Bayer precipitated particles are agglomerates of single pseudohexagonal plate-like crystallites. The structure and properties of the particles are influenced by the processes during formation: nucleation, agglomeration, crystal growth and attrition [7, 8]. During calcination the wet gibbsite loses its adhesive moisture first, further the bound water (~34 % referring to the dry hydrated material) exits. All of decomposition pathways are closed by the formation of the only thermodynamically stable oxide phase, corundum (α-Al_2O_3) [1]. The decomposition pathway is influenced by the factors of calcination. The major factors are the physicochemical properties of the initial raw (untreated) material (e.g. particle size, shape, substituting elements) and the circumstances of the heat treatment (temperature, heating rate, composition of the atmosphere, pressure) [9, 10].

The thermal decomposition reactions of aluminum-hydroxides has been reported since the middle of 20th century in a row of papers. Figure 1. summarizes the reaction pathways depending on the conditions of thermal treatment and the physical properties of particles. The following decomposition reactions are given for normal atmospheric air pressure. Dehydroxylation of gibbsite begins above the temperature of 200-300 °C. At higher temperatures different amorphous and crystalline alumina phases appear. The last step of all decomposition pathways is the formation of corundum (α-Al_2O_3). Over 200 °C a part of gibbsite loses two moles of H_2O and changes into oxi-hydroxide, as boehmite. Above 300 °C gibbsite decomposes directly into aluminum-oxide. Boehmite loses the remaining one mole of H_2O at 450-550 °C [1]. Decomposition temperatures are influenced by heating rate: the faster the temperature increase, the higher the starting temperature of decomposition is [11, 12].

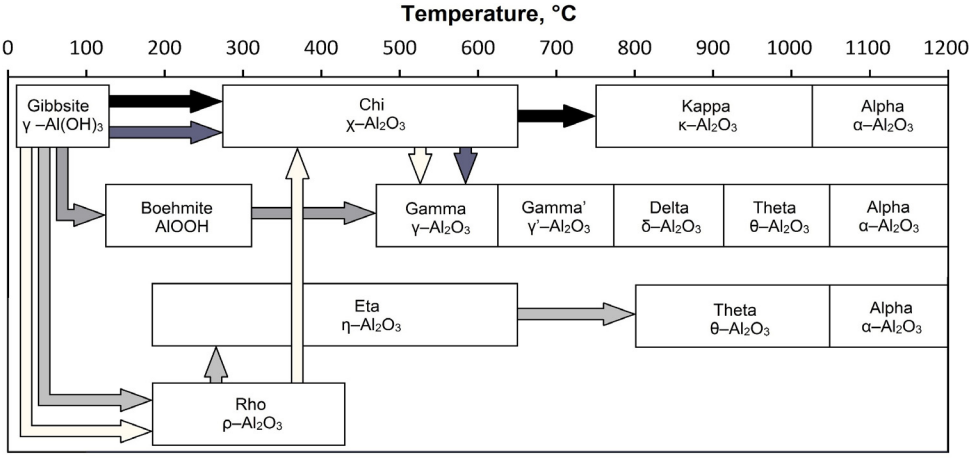

Figure 1. Thermal decomposition pathways of gibbsite, adapted from Perander [10].

Phenomenon of boehmite formation is explained by several authors, in different ways. Conditions causing higher internal steam pressure within the particle (coarse particles, high heating rate, and high concentration of water steam) favor the decomposition via boehmite. With slow heating, fine particles retard the formation of boehmite, favoring the direct decomposition into oxides [13, 14]. These predicates are prevalent in case of heat treatment at normal atmospheric pressure. If the pressure is lower (vacuum) or higher (overpressure) as normal atmospheric pressure, the decomposition processes are different [15-17]. Opposed to the above arguing, Mercury et al. [9] states that gibbsite decomposes to boehmite irrespective of particle size distribution. In case of amorphous material, the decomposition yields oxides, without boehmite formation [9, 18].

Effect of long term grinding of gibbsite is the amorphisation and appearing of gel-like hydroxide phases. The original water content of gibbsite remains invariable or slightly decreases. The product of thermal decomposition of gel-like hydroxides is amorphous oxide which transforms to crystalline form at elevated temperature [19, 20].

Several authors investigated the thermal decomposition processes of long term ground materials, like gibbsite, bayerite and boehmite [21-24].

Physical properties of alumina products applied as adsorbents, catalysts or catalyst carriers are highly influenced by decomposition processes of gibbsite [23, 25, 26]. The accompanying phenomena of dehydroxilation are in number of cases undesired. Ceramics industry utilizes boehmite when large shrinkage and porosity formation must be avoided [27, 28]. Plastics and electronics industries use increasingly boehmite as fire retardant filler, because boehmite is more stable at higher temperatures compared to gibbsite [29]. The above examples prove the necessity of knowledge expansion over gibbsite thermal decomposition processes.

Present study compares thermal decomposition of three aluminum hydroxide materials: Bayer precipitated, fine precipitated, and short term ground. All of the three samples consisted prevailingly of gibbsite. We attempted to find out, how grain and crystallite size influences the thermal decomposition processes, considering the formation of boehmite as intermediate product.

RESULTS AND DISCUSSION

1. Chemical composition and particle size of starting materials

Chemical composition of C and FP samples is shown in Table 1. As expected, only trace amounts of contaminant elements were detected. Loss on ignition values confirm the $Al(OH)_3$ composition of samples. The measured

Na_2O content is normal for these materials, as residual component from the Bayer-process. Altogether, no chemical compounds were observed that would influence the results of thermal behavior.

Particle size distribution of “original Bayer precipitated” material, CU, GU and FPU can be seen in Figure 2. The “original Bayer precipitated” sample has wide distribution of particle diameter, the size of the finest 10 % of particles is below 30 μm, while the coarsest 10 % of particles exceed 120 μm of size. Size fractionation made the mean particle size overrepresented: limits of finest and coarsest 10 % were 52 and 99 μm, respectively. Grinding reduced the median size of original material to 13 μm. Above figures of ground particle diameter are in accordance with the results of Tsuchida et al. [19]. Further milling causes only moderate decrease in particle size, but degrades the crystal structure. FPU sample has shown the finest particle distribution with median diameter at 1.9 μm.

Table 1. Chemical composition of samples

wt%	SiO_2	Al_2O_3	CaO	Na_2O	K_2O	Fe_2O_3	MnO	TiO_2	P_2O_5	L.O.I
C	0.01	65.4	0.01	0.10	0.05	0.03	0.001	n.d.	0.001	34.398
FP	0.02	65.4	0.01	0.13	0.05	0.02	0.001	n.d.	0.001	34.368
ppm	S	Cu	Zn	Pb	As	Ga	Zr	In	Ge	Sr
C	653	30	275	22	n.d	93	n.d.	n.d	n.d.	n.d
FP	468	12	178	24	n.d	91	n.d.	n.d.	n.d.	n.d

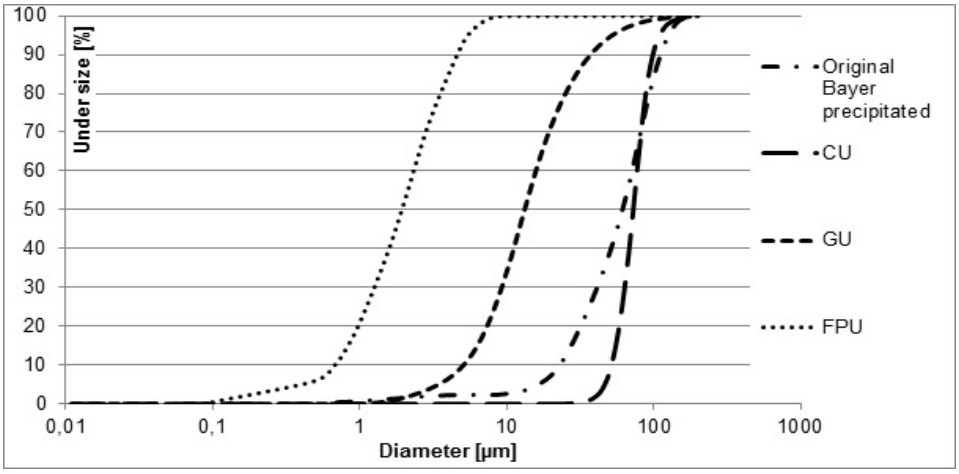

Figure 2. Cumulative particle size distribution of original Bayer precipitated, classified, ground and fine precipitated samples

2. Evaluation of experimental results

2.1. Weight loss during thermal treatment at 260 °C

Boehmite during thermal decomposition of gibbsite evolves between 200-300 °C and remains stable until 400-450 °C [9, 19, 30]. The course of boehmite evolution is followed by direct transformation of gibbsite to oxide. The intersection of the two partially overlapped processes appears between 250-270 °C depending on the conditions of heating. The temperature of heat treatment was chosen as 260 °C, according to our previous survey [31]. We have heated 10 grams of each sample in programmable furnace (Nabertherm, with ±5 °C thermal inertia) at 260 °C for 30 minutes.

Table 2 summarizes the codes of heat treated and unheated samples.

Table 2. Sample codes

Sample	Classified	Ground	Fine precipitated
unheated	CU	GU	FPU
heated	C260	G260	FP260

The weight losses of samples are 18.24 % for C, 22.57 % for G and 9.00 % for FP. The remarkable differences may be caused by different properties of sample materials. At the chosen temperature of heat treatment the coexistence of gibbsite-boehmite and gibbsite-oxide transition reactions is observable. Taken into consideration that at the above temperature the reactions are not finished, it is ascertainable that the extent of mass loss is highly influenced by residence time, properties of material (packing density, heat conductivity) and experimental conditions like water vapor pressure. Diminished mass loss during thermal treatment of FP sample can be referred to the fine sized particles and small packing density [32, 33]. Beyond the experimental and material conditions, the effect of mechanical treatment is assumable too. Largest mass loss was detectable on ground sample, suggesting that the evolved grain structure (higher porosity, flat shape) benefits the escape of water [22, 23, 34].

2.2. X-ray powder diffraction

Boehmite was not detected in the starting materials, and variable material contents without long range order were determined (Table 3). Due to a large deviation of crystallite size values, a complex peak broadening occurred. This was not readily modelled by available options in software, neither did strain refinement and modelling give a solution. As an empirical approach, two similar crystal structures were applied to fit the gibbsite peaks: one for nanocrystalline (<300 nm) and one for microcrystalline (>300 nm) fractions. Crystallite shape effects produced strong preferred

orientation for (*00l*) peaks, modelled by March-Dollase model. Minor preferred orientation was also observed and corrected for (*hk0*) peaks. The C samples gave a similar content for the <100 nm and >500 nm mean crystallite size fractions. The grinded material had mainly microcrystalline fraction, which is realistic for original Bayer process Al-hydroxide [35]. Thus, comparing C and G samples, sieving helped in uniformization of macro- to nanocrystalline fraction ratio. In a contrasting way, FP sample is dominantly nanocrystalline, according to mean crystallite sizes (Table 3A), also indicated by BET results.

Table 3. Mineralogical composition of aluminum hydroxide samples (CS_m=mean crystallite sizes in nanometer)

A						
	CU		GU		FPU	
Phase Name	wt%	CS_m [nm]	wt%	CS_m [nm]	wt%	CS_m [nm]
Gibbsite-n	44.3	78	8.6	220	7.4	270
Gibbsite	40.7	4800	75.4	2000	67.6	350
Crystallinity undetectable	14.0		16.0		25.0	
B						
Phase Name	C260		G260		FP260	
Gibbsite-n	7.2	95	10.0	55		
Gibbsite	42.9	600			62.3	350
Boehmite	27.9	55	14.0	53	8.7	60
Crystallinity undetectable	22.0		76.0		29.0	

Phases with undetectable crystallinity were observed as two separate humps (Figure 3.), attributed to the differences in chemical composition. However, the hump centered between 10 Å and 8 Å marks an angular ranger, where the main peaks of scarbroite group minerals have their main XRD peaks. Scarbroite [$Al_5(CO_3)(OH)_{13}$•$5(H_2O)$, $d_{(003)}$=8.660 Å – $I_{\%}$=100, $d_{(-102)}$=8.340 Å – $I_{\%}$=40] and hydroscarbroite [$Al_{14}(CO_3)_3(OH)_{36}$•(H_2O), $d_{(100)}$=9.000 Å – $I_{\%}$=100] are hydrated Al-hydroxide-carbonates. Our presumption is that similar compounds may appear during precipitation, in low amounts and rather low crystallite sizes, thus their presence may not be detected. In our unheated samples these broad peaks gave crystallite sizes of a few nanometers only, therefore we chose to fit them as amorphous humps. The second hump at ~4.3 Å is considered to be an amorphous phase of gibbsite composition, as not crystallized residuum of precipitation. The

amorphous content slightly increased with grinding, due to minor amorphisation. The elevated amorphous content of FP sample is derived from its technological process and is supposed to be of Al-hydroxide composition.

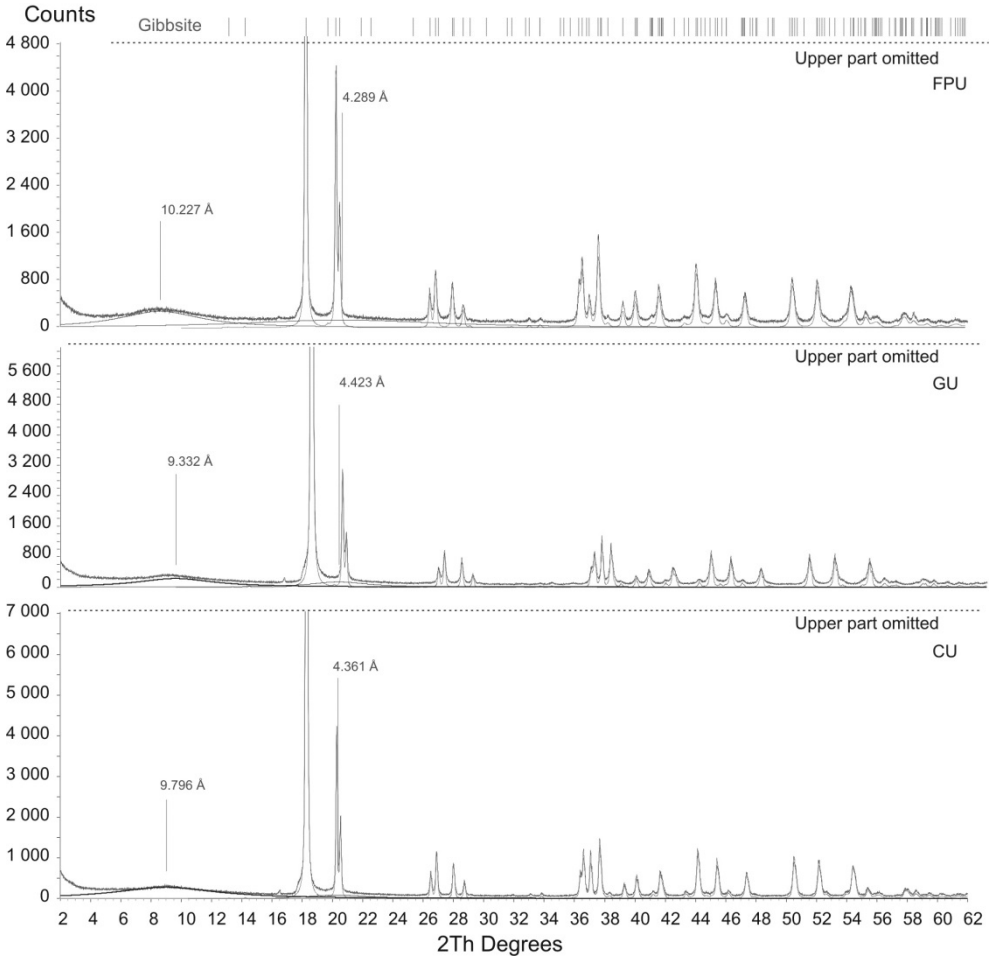

Figure 3. Rietveld-refinement results on XRD patterns for unheated samples

After heat treatment, the microcrystalline fractions were reduced or eliminated, transformed into nanocrystalline fraction (Table 3B). The amorphous content was highly raised in G sample, while only a moderate and minor increase was observed for C and FP samples, respectively. The amorphous hump at ~10Å was shifted to higher d(Å) values in G and FP, and was reduced in C sample (Figure 4). The persistence of ~10Å hump is assumed

to the presence of larger grains in unground material. The new broad peaks are due to the formation of partly dehydroxylated $Al(OH)_{3-x}$ or oxide phases. However, we did not found any similar results among available published data. Boehmite also was formed in different amounts for each material type. In C sample its amount is the highest, which is partly due to the higher nanocrystalline gibbsite content, which is readily transformed into boehmite in this stage. The boehmite to gibbsite ratio is higher in G material, but the boehmite amount is low, most of the microcrystalline and nanocrystalline gibbsite was decomposed. The lowest boehmite formation was observed in FP material, with almost all of the gibbsite being retained. To explain this behavior we have to take into account several influencing factors.

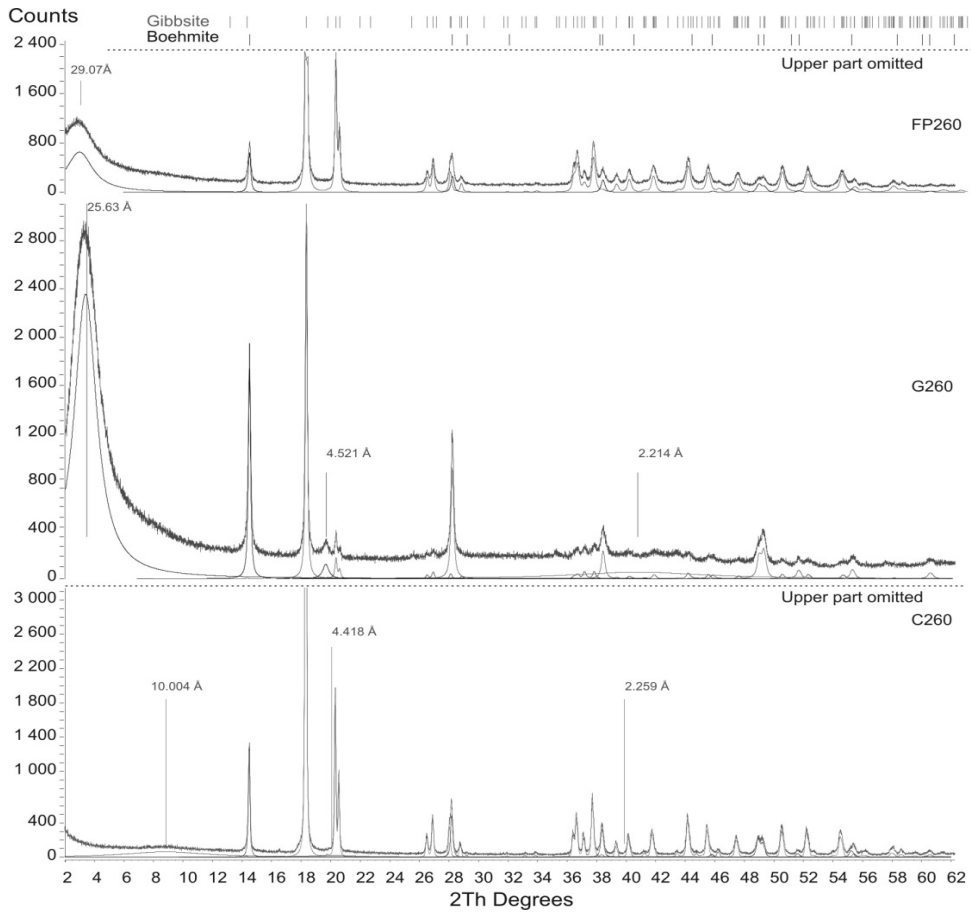

Figure 4. Rietveld-refinement results on XRD patterns for heat treated samples

The small particle diameters do not promote the hydrothermal conditions necessary for boehmite formation within the core of crystals [14, 15, 23, 36, 37]. Considerable affecting factors can be the retarded heat transfer mechanism in the volume of material and consequently the decelerated warming rate and the shorter soaking time. The finer grained the material, the more closed pores can be formed in the intergranular space, by agglomeration, reducing thermal conductivity. In the meantime, due to the increases in grain boundary ratio with decreasing grain size, and small packing densities, diffusion of heat is also slowed down [32, 33]. We must also take into account the higher amorphous content of FP sample. If the amorphous material is present as a layer on Al-hydroxide grains, by dehydration may form a coating layer, which is also inhibiting the rising of boehmite. These factors together may result in the low boehmite formation and gibbsite retaining in FP260 sample.

According to our XRD evaluations, the crystallite size also suffered variations during thermal treatment. In both C and G samples the mean crystallite size of retained gibbsite is <100 nm and the resulted boehmite gave results of ~50 nm. In FP sample, most of the microcrystalline gibbsite was retained, with high crystallite size (unaffected by heating) but the resulted boehmite also gave values of ~60 nm (Table 3B).

2.3. Thermal analysis

Individual sub-processes of thermal decomposition of gibbsite are more or less distinguishable on TG-DTA curves, depending on the conditions of analysis. Experimental curves were divided into the following four steps: I. loosing of adsorbed water (up to 200 °C); II. transformation of gibbsite to boehmite (beginning: 200-220 °C, end: 260-285 °C); III. transformation of gibbsite to oxide (beginning: 260-280 °C, end: 385-440 °C); IV. dissociation of boehmite to oxide (beginning: 435-480 °C, end: 560-595 °C). Some of the above processes are partly overlapped (step II. and step III.), making impossible the exact evaluation of data. Step I. was negligible in case of unheated samples. During step IV. not only the boehmite contained by the sample, but boehmite evolved during step II. is decomposed. Evaluated data are shown in Table 4 and Figure 5.

Step I. is only detectable on heat treated samples. Water which escapes during step I. is derived not from original sample, but adsorbed during the time passed between heat treatment and analysis. Summing the mass decrements of thermal analysis (on basis of unheated material) and mass decrement of heat treatment results in higher total loss, in case of

C260 and G260 samples, than the stoichiometric calculated (34.6 %) loss. Subtracting mass decrement during step I. from total loss yields a result approximating eligibly the theoretic mass loss.

Table 4. TG changes and DTA peak areas during thermal analysis

		Unheated			Heat treated		
		C	G	FP	C	G	FP
Step I.	TG decrement [%]	n.d.	n.d.	n.d.	2.5	3.3	1.8
	TG decrement calculated for U sample [%]				2.0	2.5	1.6
	DTA peak area [uV s/mg]				17.4	17.8	8.6
Step II.	TG decrement [%]	5.5	2.2	n.d.	n.d.	n.d.	n.d.
	TG decrement calculated for U sample [%]	-	-				
	DTA peak area [uV s/mg]	43.2	13.3				
Step III.	TG decrement [%]	21.6	25.6	30.5	14.5	9.0	21.9
	TG decrement calculated for U sample [%]	-	-	-	11.8	6.9	19.9
	DTA peak area [uV s/mg]	237.4	244.3	274.2	130.8	37.3	180.1
Step IV.	TG decrement [%]	3.9	2.9	1.5	5.3	3.7	2.7
	TG decrement calculated for U sample [%]	-	-	-	4.4	2.9	2.4
	DTA peak area [uV s/mg]	36.2	15.5	5.4	41.6	12.2	5.0
Total mass loss [%]		34.1	33.6	34.5	23.3	17.4	27.7
Total mass loss calculated for U sample [%]		-	-	-	19.1	13.5	25.2

The unheated samples contain phases considered as amorphous. Those phases exhibit crystalline hydroxide-like behavior during thermal analysis. Presence of above phases has not caused observable deviance between stoichiometric and measured weight loss, nor resulted in surplus peaks. Thermal decomposition under 200 °C can be attributed to mechanically amorphised hydroxides, and is characteristic in case of prolonged/intensive grinding [19, 22, 23]. Neither GU nor G260 samples have shown signs of grinding caused amorphisation.

Step II. is detectable only in case of untreated samples, what suggests that remaining gibbsite content of heat treated samples will not transform to boehmite. Difference between TG decrements and DTA peaks (C>G>FP) of unheated samples during Step II. indicates different amounts of boehmite evolved due to the dissimilar particle and crystalline sizes of powders.

All of samples had shown TG decrease during step III. The total mass losses of untreated samples are comparatively correspondent. Consequently the extent of step III. is influenced by boehmite evolution and decomposition (boehmite evolves at expense of gibbsite). Remaining hydroxide content, therefore mass loss during step III., of heat treated samples is affected by losses during previous decomposition processes.

Step IV. indicates the decomposition of boehmite formed during Step II. or previous heat treatment. Similarly to Step II., extent of TG decrement and DTA area during Step IV. correlates to the inclination of boehmite formation of original samples, what is influenced by particle and crystalline sizes. Largest TG decrease and DTA area belongs to C samples (heat treated and untreated too) while G samples show considerably smaller, and FP samples indicate the smallest values. This suggests that during calcination of Bayer precipitated coarse aluminum-hydroxide particles the decomposition pathway via boehmite is more significant compared to ground or fine precipitated materials. Considerable differences were not experienced between heat treated and unheated samples in extent of Step IV.

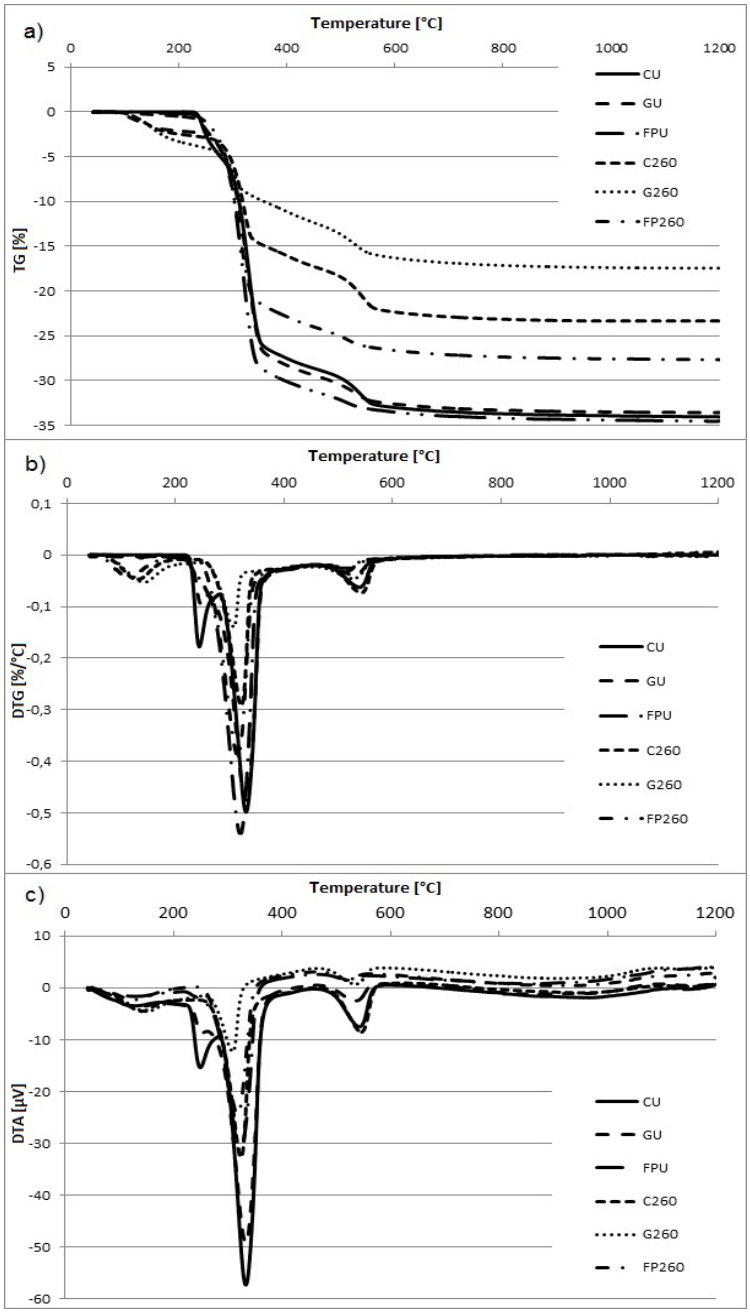

Figure 5. Thermoanalytical curves of samples: a) TG, b) DTG, c) DTA

2.4. Specific surface area

BET specific surface areas of the samples are visible on Figure 6. CU sample has the smallest value (0.12 m^2/g), while grinding increased that to 4.33 m^2/g. FPU is the finest sample (difference in particle size between FP and G is approximately one order of magnitude), the BET specific surface are of FPU is 2.96 m^2/g. It suggests that bigger surface area caused by grinding evolves not only because of attrition and emerging new surfaces, but contribution of porosity can be considerable too. Initial stage of calcination causes rapid growing of porosity and specific surface area. This is attributable to evolved water molecules escaping to the particle surface, forming slit shaped pores parallel to the 001 plane [10, 36]. As it is noticed, BET specific surface areas of C260 and FP260 samples are approximately equivalent (97.29 m^2/g and 101.24 m^2/g, respectively), while in case of G260 sample it is larger (234.34 m^2/g). It must be taken into account that heat treatment of different samples resulted in different degree of decomposition.

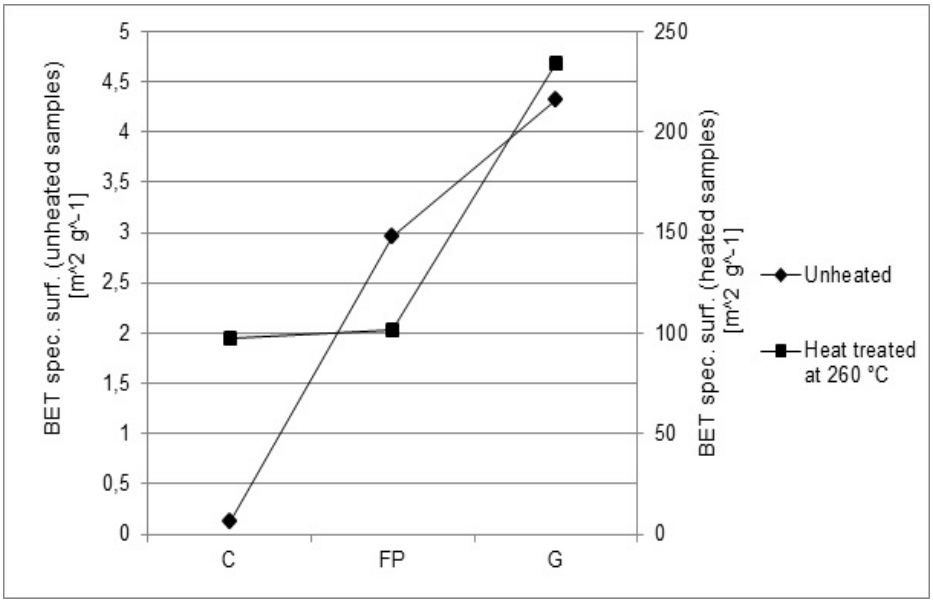

Figure 6. BET specific surface area of unheated (left axis) and heated (right axis) samples

2.5. Scanning electron microscopy

CU sample particles are agglomerates of single pseudohexagonal platy crystallites (Figure 7a). Heat treatment at 260 °C has not caused change on morphological appearance, while the long-shaped pores parallel to 001 plane are distinguishable (Figure 7b). Grinding caused considerable decrease of particle size, however particle fragments above size of 30 μm are observable too. Those relatively big particle fragments are plate like shaped, cracked along the 001 plane (Figure 7c). Craks are perceptible on the sides parallel to 001 plane of the lumps within heat treated sample (Figure 7d). Difference between particle size of GU and FPU samples is approximately one order of magnitude. Occurrence of particles with diameter above 1 μm is extremely rare in FPU. Morphological differences between FPU and FP260 samples with available method was not detectable (Figure 7e-f).

CONCLUSIONS

Both the L.O.I. values at XRF measurements and TG weight loss proved that all the samples have a $Al(OH)_3$ ($\pm$ H_2O) chemical composition, regardless of their crystalline or amorphous state. The possible presence of hydrated (and carbonated?) Al-hydroxide was indicated by XRD, considered as amorphous.

The phases with undetectable crystallinity calculated from XRD are not influencing the weight losses by heating, but in the case of FP sample it might have a role in inhibiting boehmite formation. According to TG results, the higher weight loss was recorded in FPU sample, with the lowest crystallite sizes for gibbsite. Accordingly, the lowest weight loss was observed for GU samples, with the highest microcrystalline gibbsite content.

Specific surface area is increased by grinding, due to the opening of closed nanopores by disaggregation. The highest degree of amorphous formation happened in the material with highest specific surface area, proving the importance of free grain surfaces in gibbsite decomposition.

Boehmite formation is mainly promoted by aggregate grain size and internal morphology (relevant for steam pressure generation) but also the microcrystalline nature of gibbsite, as a secondary factor.

As we could observe, thermal treatment affected the grain integrity of samples, cracking appeared on crystallographic directions, mainly in the (*001*) plane. From XRD results also a decrease in crystallite size for gibbsite is observed. This indicates, that the cracking observed by SEM is affecting the integrity of crystallites.

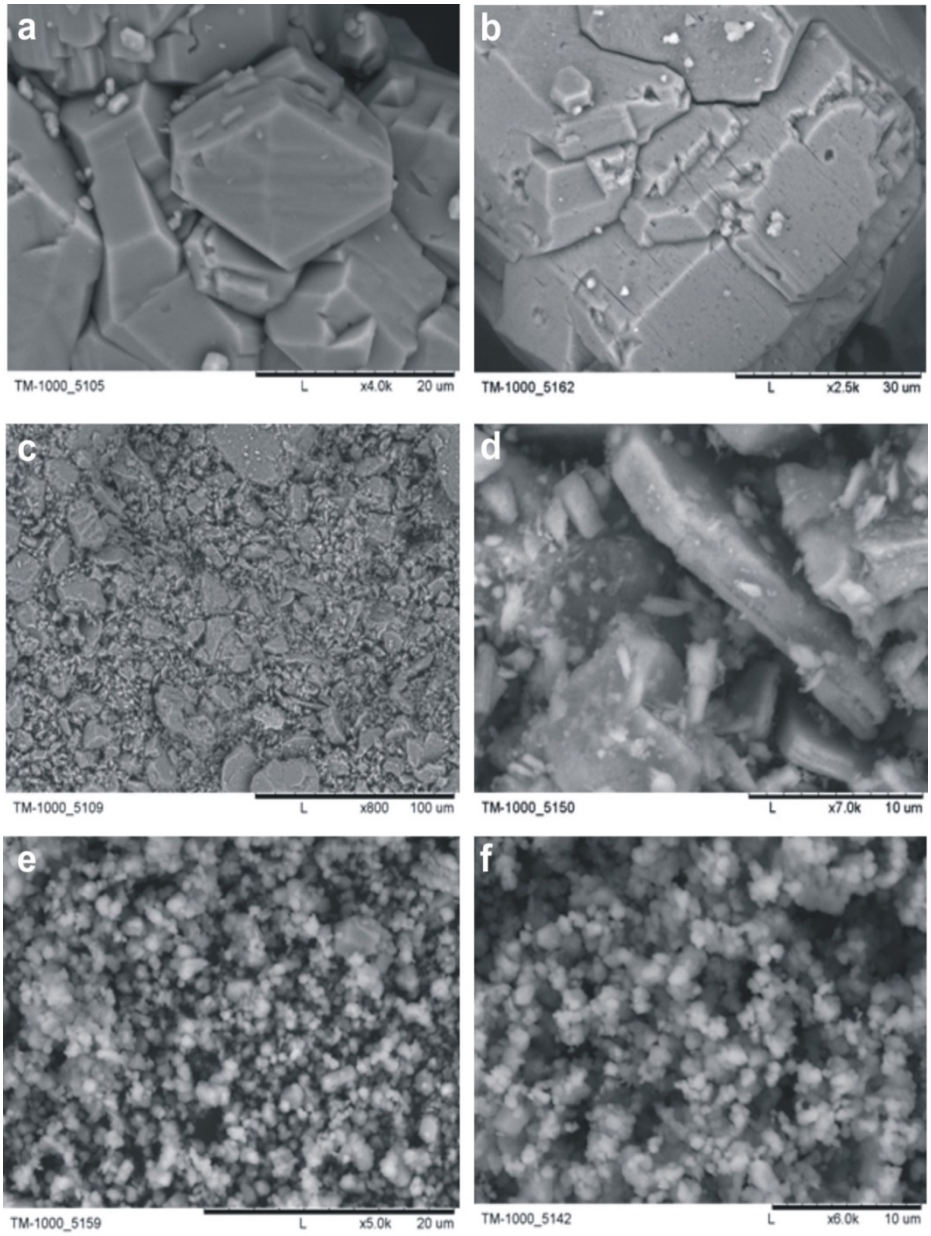

Figure 7. SEM images of samples; a) CU, b) C260, c) GU, d) G260, e) FPU, f) FP260

EXPERIMENTAL SECTION

1. Instrumentation

Particle size determinations were done on a Horiba LA-950 laser scattering particle size distribution analyzer in presence of sodium pyrophosphate solution. Samples were dispersed in ultrasonic bath for one minute before the measurement.

The chemical composition of C and FP samples was measured by X-ray Fluorescence Spectrometry (XRF, Rigaku Supermini200, WD-system, Pd source, 50kV-4nA).

X-ray powder diffraction (XRD) was performed for each material (Bruker D8 Advance, Cu-Kα source, 33 kV and 50 mA, Bragg-Brentano with Våntec-1 position sensitive detector). Measurement time of 5 minutes was allowed, to avoid rehydration of heated samples. Quantitative results were obtained by Rietveld-refinement, in Bruker TOPAS4 software, using ICSD database, unit cell parameters were refined and mean crystallite sizes determined.

Thermal analysis by simultaneous differential thermal analysis (DTA), thermogravimetry (TG) and derivative thermogravimetry (DTG) was made on a Setaram Setsys 24 instrument (heating rate 10 K min^{-1} up to 1200 °C, 55-60 mg sample, dispensed into ceramic crucible, in synthetic high flow air atmosphere). The base-line correction of DTA curves was done with measured correction data (α-Al_2O_3), smoothing of TG and DTA data was unnecessary.

Scanning electron microscopy (SEM) for morphological examinations were performed on a Hitachi TM 1000 instrument at 15 kV acceleration voltage and 10nA probe current. The powder samples were deposited on self-adhering carbon plates, without surface coating, in low vacuum chamber, to avoid morphology and aggregate structure deterioration. Back-scattered electron (BSE) images were recorded.

Specific surface area was measured on TriStar 3000 analyzer by multipoint BET method (77.35 K temperature, N_2 adsorptive, 0.3-0.5 g sample).

2. Materials

Examined materials were obtained from original Bayer precipitated, by sieving – size fractioned Bayer precipitated (C), and grinding – ground Bayer precipitated (G) aluminum hydroxide. Sieving was done in dry state between sieves with mesh size of 63 and 100 μm, shaken for 5 minutes. Size fractionation allows to avoid the disturbing effects in analytical results, caused by extremely fine and coarse particles. Ground sample was prepared in planetary mill by dry grinding (Fritsch Pulverisette 6). Six grams of C Al-hydroxide was

charged into an agate jar of 250 ml together with six agate balls (18 mm diameter). Duration of grinding was 15 minutes at a rotational speed of 500 rpm, stopped in every five minutes, to remove the adhered material from the inner wall of jar. Conditions of milling corresponded to our former experiment [31].

Also a fine precipitated (FP) aluminum hydroxide, with a finer grains size, was used in experiments, to compare its behavior with C and G. Original Bayer precipitated and fine precipitated materials were purchased from MAL Co. Ltd. Ajka Plant (Hungary). Purity of fine precipitated aluminum hydroxide (type of ALOLT 60DLS) is above 99.5 %, analyzed contaminations are SiO_2: 0.004 mass % and Fe_2O_3: 0.006 mass % (results given by MAL Co. Ltd.).

ACKNOWLEDGMENTS

The work described was carried out as part of the TÁMOP-4.2.1.B-10/2/KONV-2010-0001 project in the framework of the New Hungarian Development Plan. The authors are grateful for the help of Dr. Gábor Mucsi (grain size analysis) and Tibor Ferenczi (BET specific surface area analysis). Dr. Prof. László A. Gömze is aknowledged for his help in obtaining the SEM images.

REFERENCES

1. W.H. Gitzen, „Alumina as a Ceramic Material”, American Ceramic Society, Westerville, **1970**.
2. R. Salomão, J. Brandi, *Ceram. Int.,* **2013**, *39*, 8227.
3. R. Salomão, M.O.C. Villas Bôas, V.C. Pandolfelli, *Ceram. Int.*, **2011**, *37*, 1393.
4. L. Peng, X. Xu, Z. Lv, J. Song, M. He, Q. Wang, L. Yan, Y. Li, Z. Li, *J. Therm. Anal. Calorim.*, **2012**, *110*, 749.
5. W.J. Tseng, P. Wu, *Ceram. Int.*, **2012**, *38*, 4461.
6. W.J. Tseng, P. Wu, *Ceram. Int.*, **2012**, *38*, 2711.
7. F. Habashi, “Extractive Metallurgy of Aluminum”, in G.E. Totten, D.S. MacKenzie, “Handbook of Aluminum: Volume 2: Alloy Production and Materials Manufacturing”, Taylor & Francis, New York, Basel, **2003**.
8. A.R. Hind, K.S. Bhargava, C.S. Grocott, *Colloid. Surface*, **1999**, *146*, 359.
9. J.M.R. Mercury, P. Pena, A.H.D. Aza, D. Sheptyakov, X. Turrillas, *J. Am. Ceram. Soc.*, **2006**, *89*, 3728.
10. L.M. Perander, “Evolution of Nano- and Microstructure During the Calcination of Bayer Gibbsite to Produce Alumina”, PhD thesis, The University of Auckland, Auckland, **2010.**
11. B. Zhu, B. Fang, X. Li, *Ceram. Int.*, **2010**, *36*, 2493.

12. B. Xu, P. Smith, *Thermochim. Acta*, **2012**, *531*, 46.
13. B.K. Gan, I.C. Madsenb, J.G. Hockridge, *J. Appl. Crystallogr.*, **2009**, *42*, 697.
14. J. Rouquerol, F. Rouquerol, M. Ganteaume, *J. Catal.*, **1975**, *36*, 99.
15. J. Rouquerol, M. Ganteaume, *J. Therm. Anal.*, **1977**, *11*, 201.
16. N. Koga, S. Yamada, *Solid State Ionics*, **2004**, *172*, 253.
17. C. Novák, G. Pokol, V. Izvekov, T. Gál, *J. Therm. Anal.*, **1990**, *36*, 1895.
18. I.N. Bhattacharya, S.C. Das, P.S. Mukherjee, S. Paul, P.K. Mitra, *Scand. J. Metall.*, **2004**, *33*, 211.
19. T. Tsuchida, N. Ichikawa, *React. Solid.*, **1989**, *7*, 207.
20. J. Temuujin, K.J.D. MacKenzie, M. Schmücker, H. Schneider, J. McManus, S. Wimperis, *J. Eur. Ceram. Soc.*, **2000**, *20*, 413.
21. T.C. Alex, *J. Therm. Anal. Calorim.*, **2014**, *117*, 163.
22. K.J.D. MacKenzie, J. Temuujin, K. Okada, *Thermocim. Acta*, **1999**, *327*, 103.
23. N. Koga, *J. Therm. Anal. Calorim.*, **2005**, *81*, 595.
24. N. Koga, T. Fukagawa, H. Tanaka, *J. Therm. Anal. Calorim.*, **2001**, *64*, 965.
25. E.E. Kiss, G.C. Boskovic, *Rev. Roum. Chim.*, **2013**, *58*, 3
26. C. Dan, E.-J. Popovici, F. Imre, E. Indrea, P. Mărginean, I. Silaghi-Dumitrescu, *Studia UBB Chemia*, **2007**, *LII*, 91.
27. S. Cassiano-Gaspar, D. Bazer-Bachi, J. Chevalier, E. Lécolier, Y. Jorand, L. Rouleau, *Powder Technol.*, **2014**, *255*, 74.
28. K. Okada, T. Nagashima, Y. Kameshima, A. Yasumori, *Ceram. Int.*, **2003**, *29*, 533.
29. C.J. Oh, Y.K. Yi, S.J. Kim, T. Tran, M.J. Kim, *Powder Technol.*, **2013**, *235*, 556.
30. M. Földvári, "Handbook of thermogravimetric system of minerals and its use in geological practice", Magyar Állami Földtani Intézet, Budapest, **2011**.
31. V.Z. Baranyai, F. Kristály, I. Szűcs, *Materials Science and Engineering: A Publication of the University of Miskolc*, **2013**, *38*, 15.
32. H.W. Zhang, Q. Zhou, H.L. Xing, H. Muhlhaus, *Powder Technol.*, **2011**, *205*, 172.
33. K.C. Smith, T.S. Fisher, *Int. J. Hydrogen Energy*, **2012**, *37*, 13417.
34. K.J.D. MacKenzie, J. Temuujin, M.E. Smith, P. Angerer, Y. Kameshima, *Thermochim. Acta*, **2000**, *359*, 87.
35. D.A. Ksenofontov, Y.K. Kabalov, *Inorg. Mater.*, **2012**, *48*, 142.
36. B. Whittington, D. Ilievski, *Chem. Eng. J.*, **2004**, *98*, 89.
37. V. Balek, J. Šubrt, J. Rouquerol, P. Llewellyn, V. Zeleòák, I. M. Bountsewa, I.N. Beckman, K. Györyová, *J. Therm. Anal. Calorim.*, **2003**, *71*, 773.